Chiral Pseudo-D6h Dy(III) Single-Molecule Magnet Based on a Hexaaza Macrocycle

Jia-Hui Liu , Yi-Shu Jin , Jinkui Tang * , Cai-Ming Liu , Hui-Zhong Kou *

Posted Date: 7 April 2025

doi: 10.20944/preprints202504.0476.v1

Keywords: Chirality; Single-molecule magnet; hexaaza macrocycle; Dy; D6h

Article

Chiral Pseudo-D_{6h} Dy(III) Single-Molecule Magnet Based on a Hexaaza Macrocycle

Jia-Hui Liu [1], Yi-Shu Jin [1], Jin-kui Tang [2,*], Cai-Ming Liu [3] and Hui-Zhong Kou [1,*]

[1] Engineering Research Center of Advanced Rare Earth Materials (Ministry of Education), Department of Chemistry, Tsinghua University, Beijing 100084, China

[2] State Key Laboratory of Rare Earth Resource Utilization Changchun Institute of Applied Chemistry, Chinese Academy of Sciences, Renmin Street 5625, Changchun 130022, China

[3] Beijing National Laboratory for Molecular Sciences, Center for Molecular Science, Institute of Chemistry, Chinese Academy of Sciences, Beijing 100190, China; cmliu@iccas.ac.cn

* Correspondence: tang@ciac.jl.cn (J.-k.T.); kouhz@mail.tsinghua.edu.cn (H.Z.K.)

Abstract: A mononuclear complex $[Dy(phenN6)(HL')_2]PF_6{\cdot}CH_2Cl_2$ (H_2L' = R/S-1,1'-binaphthyl-2,2'-diphenol) with local D_{6h} symmetry was synthesized. Structural determination shows that Dy^{3+} was wrapped in the coordination cavity of the neutral hexaaza macrocyclic ligand phenN6, and the whole coordination plane was not planar. The axial positions are coordinated by two phenoxy groups of binaphthol in the trans form. The local configuration of Dy^{3+} is close to the regular hexagonal bipyramid D_{6h} configuration. The axial Dy-$O_{phenoxy}$ distances are 2.189(5) and 2.144 (5) Å, respectively, and the bond lengths of Dy-N on the equatorial plane are in the range of 2.525 (7)–2.719 (5) Å. The axial $O_{phthalmoxy}$-Dy-$O_{phthalmoxy}$ bond angle is 162.89(18)°, which deviates from the ideal linearity. Under the excitation of 320 nm, the characteristic emission peak of naphthalene ring appeared at 360 nm in the complex. The results of AC magnetic susceptibility test show obvious temperature dependence and frequency dependence in the AC magnetic susceptibility signals, typical of single-molecule magnetic behavior. The Cole-Cole curve in the temperature range of 6.0-28.0 K is fitted by the formula including Orbach and Raman relaxation mechanisms, giving the effective energy barrier U_{eff} = 300.2 K and the relaxation time $\tau_0 = 6.7\times10^{-7}$ s.

Keywords: Chirality; Single-molecule magnet; hexaaza macrocycle; Dy; D_{6h}

1. Introduction

Single-molecule magnets (SMMs), representing a significant breakthrough in nanomagnetism, integrate slow magnetization relaxation and quantum tunneling effects, and are potentially utilized in the fabrication of nanoscale devices and high-density data storage media.[1-5] Nevertheless, the operational thresholds of these materials predominantly reside in extreme cryogenic regimes, where the anisotropy barrier magnitude and blocking temperature emerge as critical determinants dictating their ambient-temperature functionality.[6-10] Lanthanide-based single-molecule magnets (Ln-SMMs) demonstrate substantial potential to promote iterative evolution in high-performance magnetic materials, that from the enhanced anisotropic magnetic moments and robust magnetic anisotropy inherent to rare-earth elements.[11-14]

The performance enhancement of Ln-SMMs fundamentally hinges on increasing magnetic anisotropy while suppressing quantum tunneling interference in relaxation dynamics.[15-18] The magnitude of magnetic anisotropy is predominantly governed by two competing factors: spin-orbit coupling (SOC) strength and electrostatic crystal field effects.[19-21] Long and his coworkers revealed that the oblate electron density distribution of Dy^{3+} ions enables strategic ligand engineering through their point-charge electrostatic model.[22] Weak isotropic equatorial coordination minimizes 4f electron cloud repulsion within the equatorial plane, whereas axial coordination of strong-field phenoxide,

 doi:10.20944/preprints202504.0476.v1

alkoxide, or siloxide auxiliary ligands maximizes axial magnetic anisotropy through optimized orbital overlap. Quantum tunneling processes can be effectively suppressed by high-symmetry crystal fields (e.g., D_{4d} D_{5h}, D_{6h} coordination geometries).[23-26] Furthermore, the rigidity of equatorial-plane ligands has been reported to mitigate quantum tunneling interference. A representative case was demonstrated by the Tang group in 2019 through a mononuclear dysprosium single-molecule magnet (Dy-SMM) with D_{6h}-symmetric coordination.[26] The equatorial plane employs a rigid hexaazamacrocyclic ligand, while the axial positions feature shortened Dy–$O_{phenoxy}$ bonds (2.21 Å) that are significantly shorter than other coordination bonds (2.35-2.50 Å), creating pronounced axial magnetic anisotropy through ligand-induced orbital compression.

The high coordination number propensity of lanthanide ions predisposes them to isotropic coordination modes, adverse to the magnetic anisotropy for Ln-SMMs. In this work, we synthesized a mononuclear complex [Dy(phenN6)(HL')$_2$]PF_6·CH_2Cl_2 (H_2L' = R/S-1,1'-binaphthyl-2,2'-diphenol) with local D_{6h} symmetry. The flexible linear cyclic polydentate ligand provides a weak coordination environment in the equatorial plane, forming a non-planar coordination sphere encapsulating Dy^{3+}. Axial positions are occupied by chiral phenoxy ligands $(HL')^-$, generating short Dy-$O_{phenoxy}$ coordination bonds. By constructing a high-symmetry D_{6h} local configuration and dominant strong axial coordination bonds, the magnetic anisotropy along the axial direction is maximized, thereby enhancing the effective energy barrier. AC magnetic susceptibility measurements reveal distinct temperature-dependent and frequency-dependent characteristics in the AC magnetic signals, typical of single-molecule magnet behavior.

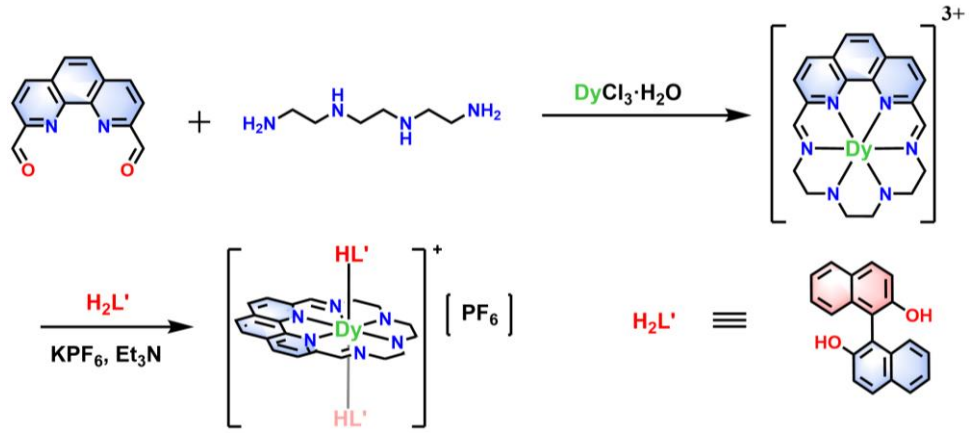

Scheme 1. Synthetic route for **1**.

2. Results and Discussion

2.1. Synthesis and Characterizations

The electrostatic repulsion model suggests that the most ideal strategy for enhancing the magnetic performance of flattened Dy^{3+} ions involves concentrating ligands in the axial direction to form a monodentate coordination compound (coordination number = 1). However, lanthanide ions exhibit diverse coordination numbers and complicated configurations, making it challenging to obtain even bidentate structures, let alone monodentate ones. In order to obtain a D_{6h} high-performance Dy(III) SMM, we adopted a two-step strategy, intentionally weakening equatorial coordinating atoms, and then strategically enhancing the axial coordination by positioning the dominant phenoxyl oxygen along the anisotropy axis.[17,21] To this end, we optimized the transverse ligand field by retaining the rigid polyaromatic framework of 1,10-phenanthroline. Through 1:1 condensation with triethylenetetramine, we synthesized a hexa-dentate cyclic neutral symmetric Schiff base ligand, phenN6. This ligand not only preserves the rigidity of phenanthroline but also employs its unique cyclic coordination cavity to encapsulate Dy^{3+} metal centers in the equatorial

 doi:10.20944/preprints202504.0476.v1

positions.[21] Simultaneously, the symmetric coordination environment ensures isotropic transverse crystal fields, effectively minimizing interference with axial anisotropy. For axial coordination, functional phenoxy oxygen ligands were employed. Through axial ligand substitution in solution, we successfully obtained a mononuclear complex **1** exhibiting local D_{6h} symmetry. The two-step synthesis of complex **1** is shown in Scheme 1.

The point chirality of ligands can be transferred through coordination to produce chiral complexes. 1,1'-bi-2-naphthol is a common chiral compound. After coordination with Dy^{3+}, a pair of chiral mononuclear complexes **1(R)** and **1(S)** are produced, which are mirror images of each other in crystal structure. The circular dichroism (CD) in acetonitrile solution further proves that they are enantiomers. As shown in Figure 1, the CD spectrum of the complex **1(R)** shows a positive Cotton effect at 221 nm and a negative Cotton effect at 235 nm, which is due to the π→π* charge transfer in the binaphthyl benzene ring. However, the CD spectrum of the complex **1(S)** shows a mirror image signal completely opposite to that of **1(R)** at the same wavelength, which indicates that **1(R)** and **1(S)** are chiral and are a pair of Dy(III) enantiomers. These results further prove that the point chirality of ligands can be effectively transferred to the whole complex structure through coordination with metal ions.

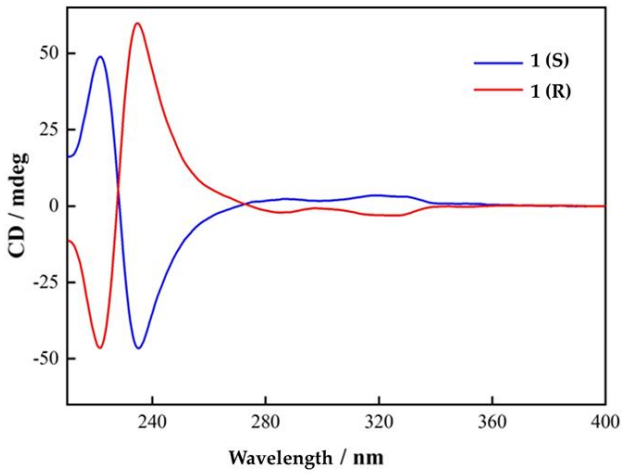

Figure 1. The CD diagram of complex **1** in acetonitrile solution ([**1**] = 5×10^{-6} M).

We tested the complexes **1(R)** and **1(S)** by TGA in order to explore their thermal stability. As can be seen from Figure S1, the sample slowly loses the lattice solvent CH_2Cl_2 from room temperature, and above 185 °C solvent completely leaves (weight loss is 4.5 %). Then in the temperature range of 185-207 °C, HPF_6 was completely removed (the weight loss of 8.3 %). When the temperature rises above 253 °C, the complex begins to decompose.

As shown in Figure S2, the infrared spectrum of complex **1** shows a strong absorption peak at 1600 cm^{-1}, which may be caused by the stretching vibration of Schiff base ligand C=N, while a strong absorption peak at 830 cm^{-1} is attributed to the P-F stretching vibration in PF_6^- ion.

Figure 2 shows the fluorescence spectra of complexes **1(R)** and **1(S)** in acetonitrile solution with excitation wavelength of 320 nm. It can be seen that they all have tiny shoulder peaks around 400 nm, which are derived from the rigid aromatic ring of equatorial plane ligands. 1,1'-binaphthyl-2,2'-diphenol is a good fluorescent chromophore, and the dihedral angle of its monomer is close to 90°, which can effectively prevent intermolecular π-π stacking, thus obtaining strong fluorescence emission. Complex **1(R/S)** has the maximum emission peak at 360 nm, which is the characteristic emission peak of naphthalene ring itself.

 doi:10.20944/preprints202504.0476.v1

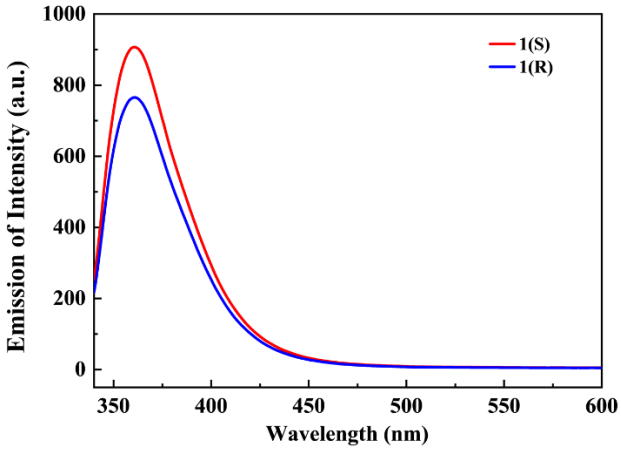

Figure 2. Fluorescence emission spectra of complexes **1** in acetonitrile (1×10^{-5} M).

2.2. Structure

Mononuclear complex **1(R)** and **1(S)** crystallize in polar space group *P*1, as shown in Figure 3. The direction of chiral helix corresponding to S/R can be determined by the orientation of uncoordinated phenol oxygen bond in 1,1'-binaphthyl-2,2'-diphenol. The independent asymmetric unit contains a Dy^{3+} ion, a neutral cyclic ligand (phenN6), two negative monovalent axial ligands $(HL')^-$, a charge-balancing anion PF_6^- and a lattice solvent CH_2Cl_2. As we designed, Dy^{3+} was indeed wrapped in the coordination cavity composed of hexaaza N_6, and the rigid limitation of o-phenanthroline made the whole equatorial position coplanar at the head, while the flexible aliphatic amine chain at the tail deviated from the equatorial plane upon the coordination (N5), which made the equatorial coordination macrocycle not coplanar. Similar situation occurs to less distorted $[Dy(bpyN6)(Ph_3SiO)_2](BPh_4)$ and $[Dy(phenN6)(Ph_3SiO)_2](PF_6)$. [17,21] The axial positions are occupied by the phenoxy group in binaphthol. According to the SHAPE calculation (version 2.1), the local configuration of Dy^{3+} is close to the compressed hexagonal bipyramidal D_{6h} configuration), and the deviation parameter is 5.478 (Table S3). The axial Dy-$O_{phenoxy}$ distances are 2.189(5) and 2.144 (5) Å, respectively, while the bond lengths of Dy-N on the equatorial plane are in the range of 2.525(7)–2.719(5) Å, which is obviously longer than the axial Dy-$O_{phenoxy}$ bond length. The axial $O_{phenoxy}$-Dy-$O_{phenoxy}$ bond angle of 162.89(18)° markedly deviates from the ideal linearity, which might be related to the spatial hindrance induced by the nonplanarity of the equatorial ligand phenN6. At the same time, the free CH_2Cl_2 and PF_6^- are situated in the crystal lattice (Figure 4), and form abundant weak intermolecular interactions. The nearest intermolecular Dy---Dy distance is 9.224 Å.

 doi:10.20944/preprints202504.0476.v1

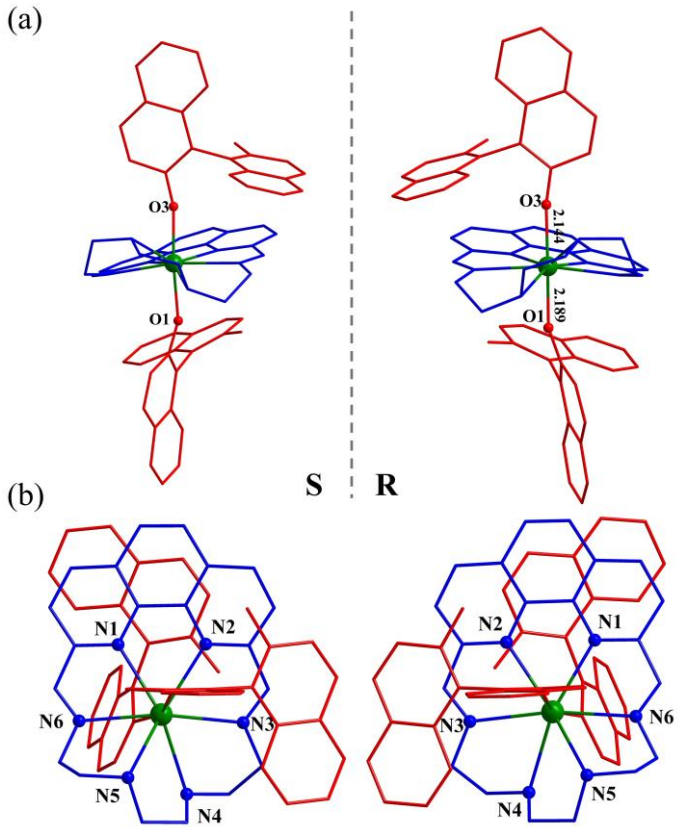

Figure 3. The crystal structure diagrams of complexes **1(S)** and **1(R)**: (a) Side view; (b) Top view. The lattice solvents and hydrogen atoms are ignored for clarity.

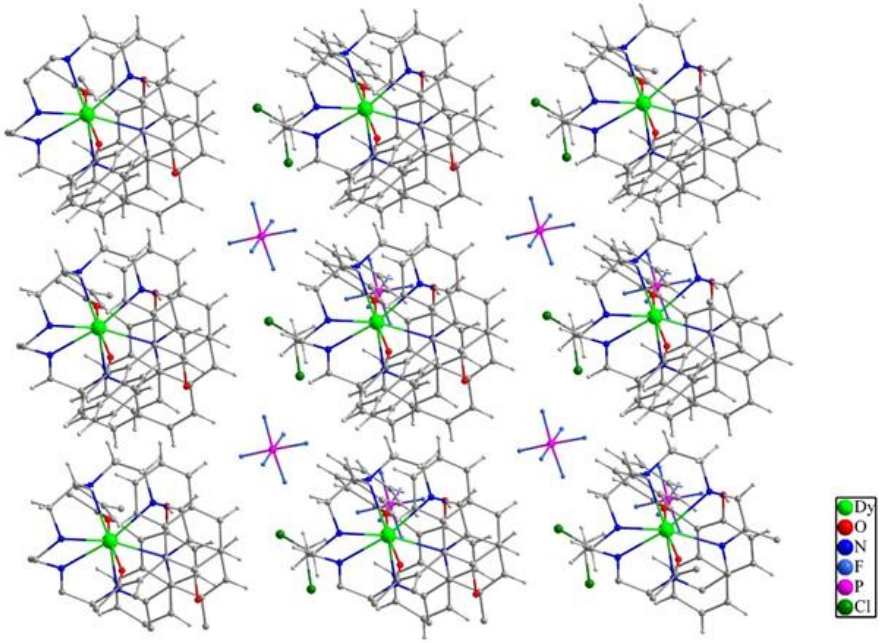

Figure 4. The molecular stacking diagram of complex **1(R)**.

 doi:10.20944/preprints202504.0476.v1

2.3. Magnetism

Variable-temperature magnetic susceptibility measurements for complex **1** were conducted under a 1000 Oe dc field across the 2-300 K range. As shown in Figure 5a, the room-temperature $\chi_M T$ value of 13.9 $cm^3 \cdot mol^{-1} \cdot K$ is close to the theoretical value (14.17 $cm^3 \cdot mol^{-1} \cdot K$) for a non-interacting Dy^{3+} ion. The $\chi_M T$ profile of mononuclear complex **1** remains nearly constant upon cooling before gradually decreasing to a minimum of 11.79 $cm^3 \cdot mol^{-1} \cdot K$ at 2 K, indicative of weak intermolecular antiferromagnetic interactions between Dy^{3+} centers. The magnetization curve of complex **1** at 2.0 K (Figure 5b) shows that the magnetization in the region of 0-1.0 T increases nearly linearly with the increase of external magnetic field, and then gradually to 5.6 $N\beta$ at 5.0 T, which is far lower than the theoretical saturation value of 10 $N\beta$ of rare earth Dy(III) ion complexes. As shown in Figure 5b, complex **1** has a small hysteresis loop at 1.9 K without residual magnetization at the external zero magnetic field.

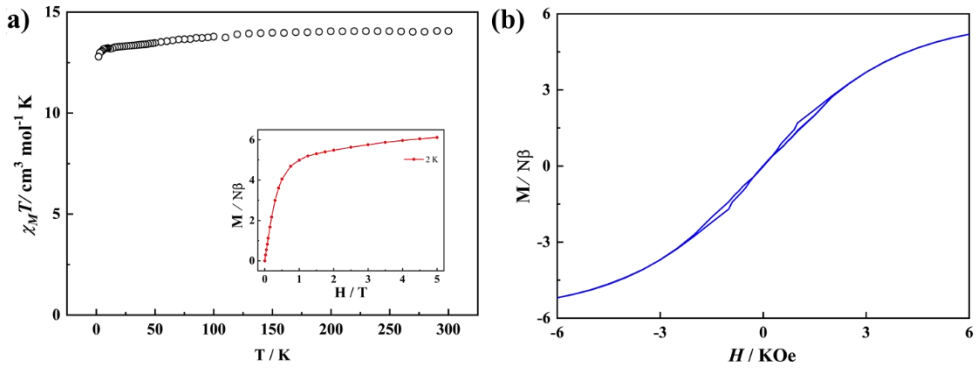

Figure 5. (a) The temperature-dependent molar magnetic susceptibility ($\chi_M T$) under a DC field of 1000 Oe, and the internal diagram shows the magnetization at a variable field of 2 K; (b) hysteresis loop at 1.9 K.

The temperature-dependent out-of-phase alternating current (ac) magnetic susceptibility of complex **1** under zero dc field is shown in Figure 6(a). The presence of non-zero χ'' signals across the 10–997 Hz range, in the absence of distinct peaks, suggests significant quantum tunneling of magnetization (QTM) within the molecular framework. To mitigate this effect, field-dependent ac susceptibility measurements were conducted at 10 K and 997 Hz to identify the optimal suppressing dc field. As revealed in Figure 6(b), the χ'' response exhibits a maximum near 1800 Oe, indicating effective QTM suppression at this field. Subsequent ac susceptibility tests were thus performed under an applied 1800 Oe dc field.

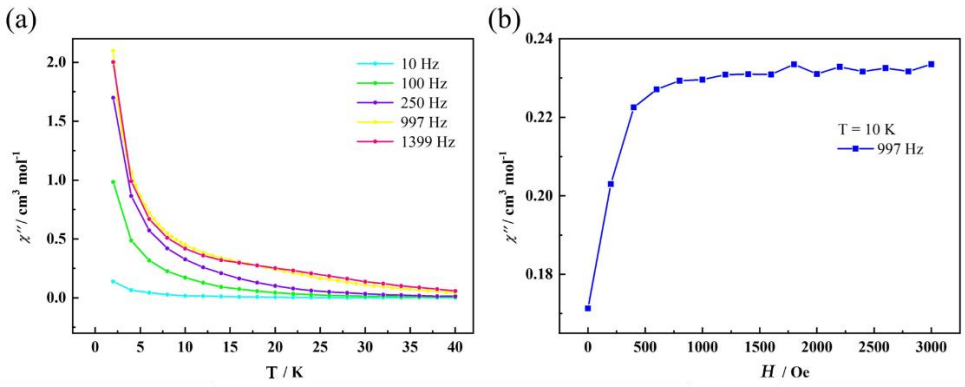

Figure 6. (a) Temperature-dependent out-of-phase alternating current (ac) magnetic susceptibility of complex **1** under zero applied dc field; (b) Field-dependent response at 10 K and 997 Hz.

 doi:10.20944/preprints202504.0476.v1

Figure 7 demonstrates pronounced temperature- and frequency-dependent out-of-phase (χ_M'') ac susceptibility signals for **1**, characteristic of single-molecule magnet (SMM) behavior. Cole-Cole plots between 6.0–28.0 K (Fig. 7c) display semicircular profiles that were satisfactorily fitted using the generalized Debye model (Table S4). The small distribution parameters ($\alpha < 0.17$) confirm a narrow relaxation time distribution, consistent with a single dominant relaxation pathway.

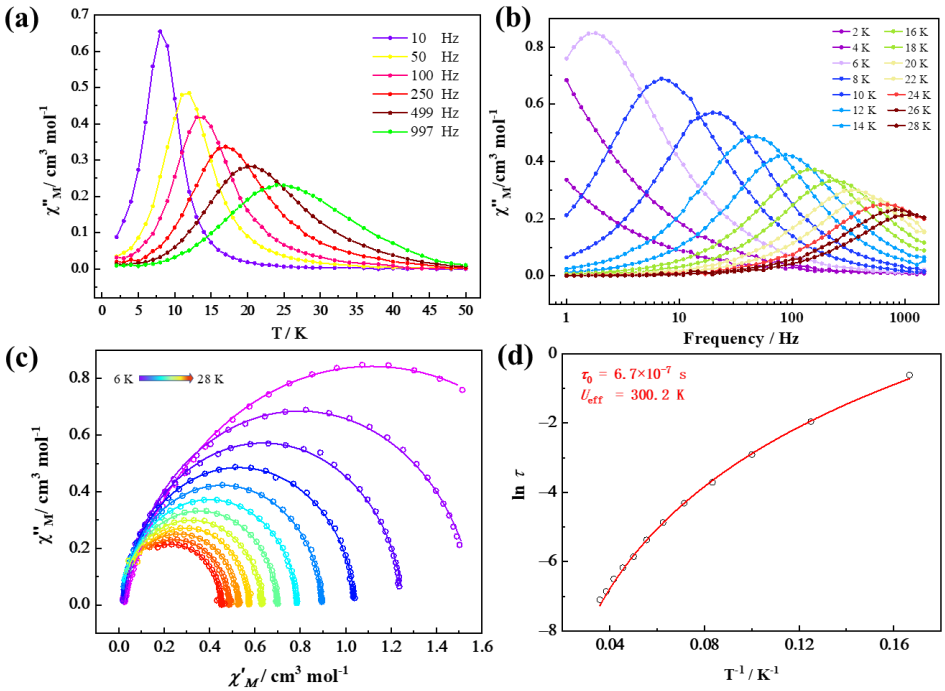

Figure 7. The dynamic magnetic behavior of complex **1** under the applied DC field of 1800 Oe: (a) the curves of temperature dependent imaginary AC susceptibility χ_M''; (b) frequency-dependent χ_M'' curves; (c) Core-Core plots, and the solid lines are the fitting results; (d) ln τ is plotted against T^{-1}, and the solid line is the fitting result.

Arrhenius analysis of the extracted relaxation times (lnτ vs. T^{-1}) reveals two distinct regimes: (i) A linear high-temperature region ($T > 15$ K) governed by the Orbach process, and (ii) a curved low-temperature region ($T < 15$ K) dominated by a Raman relaxation mechanism. Consequently, the entire temperature range was fitted using Equation $\tau^{-1} = CT^n + \tau_0^{-1} \exp\left(-\frac{U_{\text{eff}}}{k_B T}\right)$ incorporating both Orbach and Raman relaxation mechanisms, yielding the parameters: $n = 4.24$, $C = 0.001$ s^{-1}·K^{-n}, $U_{\text{eff}} = 300.2$ K, and $\tau_0 = 6.7 \times 10^{-7}$ s.

For Dy(III) single-molecule magnets, the magnitude of the effective energy barrier is primarily determined by the coordination environment of the rare-earth ion. Subtle alterations in local coordination geometry and variations in charge distribution can both induce modifications in single-molecule magnetic properties.[27,28] Recent reports on Dy-SMMs (37 cases) with the D_{6h} spatial configuration show that they possess the U_{eff} values in the range of 35-2437 K (Table S5).[17-21,26,29-39] It is well documented that for mononuclear D_{6h}-Dy single-molecule magnets, the rigidity and electrical properties of the equatorial ligands, the electronegativity of the coordination atoms and the steric hindrance of the axial ligands will change the structure and local coordination configuration (coplanarity) of the complex, and then alter the strength of the crystal field around Dy(III), thus regulating the magnetic anisotropy of Dy(III). Comparison of the magnetic properties for D_{6h} high-performance Dy-SMMs in Table S5 suggests that the axial O-Dy-O bond angle plays the most critical role, i.e. larger bond angles correspond to better magnetic anisotropy and higher U_{eff}. Besides, the coplanarity, electrical neutrality and strong electronegativity of coordination atoms play a favorable secondary role. In complex **1**, the Dy^{3+} center adopts a compressed D_{6h} configuration with a neutral hexaaza macrocyclic ligand, showing a medium U_{eff} among the similar pseudo-D_{6h} Dy-SMMs (Table

 doi:10.20944/preprints202504.0476.v1

S5). The small axial O-Dy-O bond angle of 162.89(18)º should be responsible for the situation. Previous theoretical calculation results indicate that the large deviation from ideal D_{6h} usually brings about the QTM process occurred in the first excited state, which leads to the failure of the energy barrier flip to to the second excited state, and finally a small effective energy barrier. In contrast, ideal D_{6h} could make the anisotropic axis of the first excited state and even the higher excited states coincide with the ground state, and then the QTM in the first or higher excited states can be effectively suppressed, thus significantly improving the effective energy barrier.[31]

3. Materials and Methods

3.1. Synthesis and Preparations

All of the reagents were commercially available and were used without further purification.

3.1.1. Synthesis of the Precursor phenN6-Dy

1.18 g (5 mmol) of 1,10-o-phenanthroline-2,9-dicarbaldehyde was dissolved in 30 mL of hot ethanol, then 800 μL (5 mmol) of triethylenetetramine was added, and the reaction system began to slowly produce turbidity, then 1.92 g (5 mmol) of dysprosium chloride hexahydrate was added. The mixture was heated to reflux for 6 h. After the reaction, a large amount of light brown precipitate was produced at the bottom of the round-bottomed flask. The reaction product was collected by suction filtration and was repeatedly washed with ice ethanol. Finally, the potential coordination solvent was removed by vacuum drying at 80 °C for 5 h, and finally about 1.8 g of brown powder phenN6-Dy was obtained with a yield of about 65%.

3.1.2. Synthesis of Complex $[Dy(phenN6)(HL')_2]PF_6{\cdot}CH_2Cl_2$ (1R/1S)

Precursors phenN6-Dy (0.05 mmol), R/S-1,1'-binaphthyl-2,2'-diphenol (H_2L', 0.1 mmol), KPF_6 (0.1 mmol) and triethylamine (0.1 mmol) were respectively added into 10 mL of dichloromethane solvent, and then 10 mL of deionized water was added into the mixed system under stirring at room temperature. Subsequently, the reaction system was refluxed for 2 h. The solution was allowed to cool at room temperature. The dichloromethane layer was separated and filtered, and the crimson filtrate was allowed to stand and evaporate slowly in a small bottle with a hole. Two days later, red flaky crystals were precipitated with a yield of about 53 % (based on the amount of precursor phenN6-Dy).

3.2. Physical Measurements

Single crystal X-ray data were collected by Rigaku SuperNova, Dual, Cu at zero and AtlasS2. Use Olex2 1.3 program to solve the structure, and use the full matrix least square method based on F^2 to refine it with the method of SHEXL-2018/3. Hydrogen atoms are added geometrically and refined by riding model. The temperature- and field-dependent magnetic susceptibility was measured by MPMS XL5 SQUID magnetometer of Quantum Design Company. Infrared spectra (KBr tablet) in the range of 400 ~ 4000 cm^{-1} were recorded on WQF 510A FTIR equipment, and the scanning interval was 2 cm^{-1}. TU-1901 spectrophotometer was used to measure the ultraviolet-visible absorption spectra in the range of 280 ~ 600 nm, and the scanning interval was 0.5 nm. The photoluminescence spectrum was measured by Lengguang F98 fluorescence spectrophotometer. The scanning speed is 1000 nm/min and the scanning interval is 1 nm. The circular dichroism (CD) spectrum was measured by JASCO J-1500 spectrometer.

4. Conclusions

A chiral mononuclear complex $[Dy(phenN6)(HL')_2]PF_6{\cdot}CH_2Cl_2$ (H_2L' = R/S-1,1'-binaphthyl-2,2'-diphenol) with local D_{6h} symmetry was successfully constructed. The short Dy–$O_{phenoxy}$ coordination bonds formed through axial coordination of chiral HL'^- ligands effectively enhance the magnetic

 doi:10.20944/preprints202504.0476.v1

anisotropy. AC magnetic susceptibility measurements unambiguously confirm the single-molecule magnet behavior with the effective energy barrier of 300.2 K. This work reemphasizes that perfect D_{6h} coordination configuration of Dy(III) is in favor of high-performance Dy-SMMs.

Supplementary Materials: The following supporting information can be downloaded at the website of this paper posted on Preprints.org, Figure S1: The thermogravimetric curves of complex 1(R/S); Figure S2: Infrared spectrum of complex 1(R/S); Table S1: Crystal data of complexes **1R/S**; Table S2: Selected Bond Distances (Å) and Bond Angles (°) in Complexes 1(R) and 1(S); Table S3: Coordination Geometry Calculated by SHAPE 2.1 for Complex 1R; Table S4: Core-Core Fitting parameters under 1800 Oe dc Field for complex 1; Table S5: Structural Information and the Effective Energy Barrier for D_{6h} Dy(III) SMMs.

Author Contributions: Conceptualization and formal analysis, J.-H.L. and Y.-S.J.; writing—original draft preparation, J.-H.L.; writing—review and editing, supervision, project administration and funding acquisition, H.-Z.K., C.-M.L. and J.k.T. All authors have read and agreed to the published version of the manuscript.

Funding: This research was funded by the National Natural Science Foundation of China, grant numbers 22271171, 21971142 and 92261103.

Data Availability Statement: The original contributions presented in this study are included in the article/supplementary material. Further inquiries can be directed to the corresponding author (H.-Z.K.).

Conflicts of Interest: The authors declare no conflicts of interest.

References

1. Chipman, J. A.; Berry, J. F., Paramagnetic Metal–Metal Bonded Heterometallic Complexes. *Chem. Rev.* **2020,** *120* (5), 2409-2447.
2. Guo, F.-S.; Bar, A. K.; Layfield, R. A., Main Group Chemistry at the Interface with Molecular Magnetism. *Chem. Rev.* **2019,** *119* (14), 8479-8505.
3. Kragskow, J. G. C.; Mattioni, A.; Staab, J. K.; Reta, D.; Skelton, J. M.; Chilton, N. F., Spin–phonon coupling and magnetic relaxation in single-molecule magnets. *Chem. Soc. Rev.* **2023,** *52* (14), 4567-4585.
4. Zakrzewski, J. J.; Liberka, M.; Wang, J.; Chorazy, S.; Ohkoshi, S.-i., Optical Phenomena in Molecule-Based Magnetic Materials. *Chem. Rev.* **2024,** *124* (9), 5930-6050.
5. Cavallini, M.; Gomez-Segura, J.; Ruiz-Molina, D.; Massi, M.; Albonetti, C.; Rovira, C.; Veciana, J.; Biscarini, F., Magnetic Information Storage on Polymers by Using Patterned Single-Molecule Magnets. *Angew. Chem. Int. Ed.* **2005,** *44* (6), 888-892.
6. Wang, C.; Meng, Y.-S.; Jiang, S.-D.; Wang, B.-W.; Gao, S., Approaching the uniaxiality of magnetic anisotropy in single-molecule magnets. *Sci. China Chem.* **2023,** *66* (3), 683-702.
7. Damgaard-Møller, E.; Krause, L.; Tolborg, K.; Macetti, G.; Genoni, A.; Overgaard, J., Quantification of the Magnetic Anisotropy of a Single-Molecule Magnet from the Experimental Electron Density. *Angew. Chem. Int. Ed.* **2020,** *59* (47), 21203-21209.
8. Gao, C.; Genoni, A.; Gao, S.; Jiang, S.; Soncini, A.; Overgaard, J., Observation of the asphericity of 4f-electron density and its relation to the magnetic anisotropy axis in single-molecule magnets. *Nature Chem.* **2020,** *12* (2), 213-219.
9. Raza, A.; Perfetti, M., Electronic structure and magnetic anisotropy design of functional metal complexes. *Coord. Chem. Rev.* **2023,** *490*, 215213.
10. Bar, A. K.; Pichon, C.; Sutter, J.-P., Magnetic anisotropy in two- to eight-coordinated transition–metal complexes: Recent developments in molecular magnetism. *Coord. Chem. Rev.* **2016,** *308*, 346-380.
11. Ding, Y.-S.; Chilton, N. F.; Winpenny, R. E. P.; Zheng, Y.-Z., On Approaching the Limit of Molecular Magnetic Anisotropy: A Near-Perfect Pentagonal Bipyramidal Dysprosium(III) Single-Molecule Magnet. *Angew. Chem. Int. Ed.* **2016,** *55* (52), 16071-16074.
12. Guo, Y.-N.; Xu, G.-F.; Guo, Y.; Tang, J., Relaxation dynamics of dysprosium(III) single molecule magnets. *Dalton Trans.* **2011,** *40* (39), 9953-9963.
13. Deng, W.; Du, S.-N.; Ruan, Z.-Y.; Zhao, X.-J.; Chen, Y.-C.; Liu, J.-L.; Tong, M.-L., Aggregation-induced suppression of quantum tunneling by manipulating intermolecular arrangements of magnetic dipoles. *Aggregate* **2024,** *5* (2), e441.
14. Reta, D.; Kragskow, J. G. C.; Chilton, N. F., Ab Initio Prediction of High-Temperature Magnetic Relaxation Rates in Single-Molecule Magnets. *J. Am. Chem. Soc.* **2021,** *143* (15), 5943-5950.
15. Blagg, R. J.; Ungur, L.; Tuna, F.; Speak, J.; Comar, P.; Collison, D.; Wernsdorfer, W.; McInnes, E. J. L.; Chibotaru, L. F.; Winpenny, R. E. P., Magnetic relaxation pathways in lanthanide single-molecule magnets. *Nature Chem.* **2013,** *5* (8), 673-678.

 doi:10.20944/preprints202504.0476.v1

16. Guo, F.-S.; Day, B. M.; Chen, Y.-C.; Tong, M.-L.; Mansikkamäki, A.; Layfield, R. A., Magnetic hysteresis up to 80 kelvin in a dysprosium metallocene single-molecule magnet. *Science* **2018,** *362* (6421), 1400-1403.
17. Jia, S.; Zhu, X.; Ying, B.; Dong, Y.; Sun, A.; Li, D.-f., Macrocyclic Hexagonal Bipyramidal Dy(III)-Based Single-Molecule Magnets with a D_{6h} Symmetry. *Cryst. Growth Des*. **2023**, *23 (9)*, 6967–6973.
18. Liu, S.; Gil, Y.; Zhao, C.; Wu, J.; Zhu, Z.; Li, X. L.; Aravena, D.; Tang, J., A conjugated Schiff-base macrocycle weakens the transverse crystal field of air-stable dysprosium single-molecule magnets. *Inorg. Chem. Front*. **2022**, *9*, 4982–4989.
19. Wu, J.; Li, J.; Yang, Q.; Liu, D.; Tang, J.; Zhang, B., Fine-Tuning the Anisotropies of Air-Stable Single-Molecule Magnets Based on Macrocycle Ligands. *Inorg. Chem.* **2025,** *64* (2), 999-1006.
20. Cai, X.; Cheng, Z.; Wu, Y.; Jing, R.; Tian, S.-Q.; Chen, L.; Li, Z.-Y.; Zhang, Y.-Q.; Cui, H.-H.; Yuan, A., Tuning the Equatorial Negative Charge in Hexagonal Bipyramidal Dysprosium(III) Single-Ion Magnets to Improve the Magnetic Behavior. *Inorg. Chem*. **2022**, *61 (8)*, 3664–3673.
21. Armenis, A. S.; Mondal, A.; Giblin, S. R.; Alexandropoulos, D. I.; Tang, J.; Layfield, R. A.; Stamatatos, T. C., 'Kick-in the head': high-performance and air-stable mononuclear Dy^{III} single-molecule magnets with pseudo-D_{6h} symmetry from a [1+1] Schiff-base macrocycle approach. *Inorg. Chem. Front*. **2025,** *12* (3), 1214-1224.
22. Rinehart, J. D.; Long, J. R., Exploiting single-ion anisotropy in the design of f-element single-molecule magnets. *Chem. Sci.* **2011,** *2* (11), 2078-2085.
23. Long, J.; Tolpygin, A. O.; Mamontova, E.; Lyssenko, K. A.; Liu, D.; Albaqami, M. D.; Chibotaru, L. F.; Guari, Y.; Larionova, J.; Trifonov, A. A., An unusual mechanism of building up of a high magnetization blocking barrier in an octahedral alkoxide Dy^{3+}-based single-molecule magnet. *Inorg. Chem. Front.* **2021,** *8* (5), 1166-1174.
24. Li, M.; Wu, H.; Xia, Z.; Ungur, L.; Liu, D.; Chibotaru, L. F.; Ke, H.; Chen, S.; Gao, S., An Inconspicuous Six-Coordinate Neutral Dy^{III} Single-Ion Magnet with Remarkable Magnetic Anisotropy and Stability. *Inorg. Chem.* **2020,** *59* (10), 7158-7166.
25. Ding, Y.-S.; Yu, K.-X.; Reta, D.; Ortu, F.; Winpenny, R. E. P.; Zheng, Y.-Z.; Chilton, N. F., Field- and temperature-dependent quantum tunnelling of the magnetisation in a large barrier single-molecule magnet. *Nature Commun.* **2018,** *9* (1), 3134.
26. Zhu, Z.; Zhao, C.; Feng, T.; Liu, X.; Ying, X.; Li, X.-L.; Zhang, Y.-Q.; Tang, J., Air-Stable Chiral Single-Molecule Magnets with Record Anisotropy Barrier Exceeding 1800 K. *J. Am. Chem. Soc.* **2021,** *143* (27), 10077-10082.
27. Liu, M.-J.; Wu, S.-Q.; Li, J.-X.; Zhang, Y.-Q.; Sato, O.; Kou, H.-Z., Structural Modulation of Fluorescent Rhodamine-Based Dysprosium(III) Single-Molecule Magnets. *Inorg. Chem.* **2020,** *59* (4), 2308-2315.
28. Jin, Y.-S.; Yu, K.; Zhang, N.; Zhang, Y.-Q.; Liu, C.-M.; Kou, H.-Z., From dinuclear to two-dimensional Dy(III) complexes: single crystal–single crystal transformation and single-molecule magnetic behavior. *J. Mater. Chem. C* **2023,** *11* (4), 1550-1559.
29. Canaj, A. B.; Dey, S.; Martí, E. R.; Wilson, C.; Rajaraman, G.; Murrie, M., Insight into D_{6h} Symmetry: Targeting Strong Axiality in Stable Dysprosium(III) Hexagonal Bipyramidal Single-Ion Magnets. *Angew. Chem. Int. Ed.* **2019,** *58* (40), 14146-14151.
30. Li, Z.-H.; Zhai, Y.-Q.; Chen, W.-P.; Ding, Y.-S.; Zheng, Y.-Z., Air-Stable Hexagonal Bipyramidal Dysprosium(III) Single-Ion Magnets with Nearly Perfect D_{6h} Local Symmetry. *Chem. Eur. J.* **2019,** *25* (71), 16219-16224.
31. Xu, W.-J.; Luo, Q.-C.; Li, Z.-H.; Zhai, Y.-Q.; Zheng, Y.-Z., Bis-Alkoxide Dysprosium(III) Crown Ether Complexes Exhibit Tunable Air Stability and Record Energy Barrier. *Adv. Sci.* **2024,** *11* (17), 2308548.
32. Zhao, C.; Zhu, Z.; Li, X.-L.; Tang, J., Air-stable chiral mono- and dinuclear dysprosium single-molecule magnets: steric hindrance of hexaazamacrocycles. *Inorg. Chem. Front.* **2022,** *9* (16), 4049-4055.
33. Jin, Y.-S.; Liu, C.-M.; Zhang, Y.-Q.; Kou, H.-Z., Trinuclear Dy(III) Single-Molecule Magnets with Two-Step Relaxation, *Chin. J. Chem*. **2023**, *41*, 2641−2647.
34. Zhu, Z.; Zhao, C.; Zhou, Q.; Liu, S.; Li, X.-L.; Mansikkamäki, A.; Tang, J., Air-Stable Dy(III)-Macrocycle Enantiomers: From Chiral to Polar Space Group. *CCS Chem.* **2022,** *4* (12), 3762-3771.
35. Li, J.; Gómez-Coca, S.; Dolinar, B. S.; Yang, L.; Yu, F.; Kong, M.; Zhang, Y.-Q.; Song, Y.; Dunbar, K. R., Hexagonal Bipyramidal Dy(III) Complexes as a Structural Archetype for Single-Molecule Magnets. *Inorg. Chem*. **2019**, *58*, 2610−2617.
36. Ding, Y. S.; Blackmore, W. J. A.; Zhai, Y, Q.; Giansiracusa, M. J.; Reta, D, Vitorica-Yrezabal, I.; Winpenny, R. E. P.; Chilton, N. F.; Zheng, Y. Z., Studies of the Temperature Dependence of the Structure and Magnetism of a Hexagonal-Bipyramidal Dysprosium(III) Single Molecule Magnet. *Inorg. Chem*. **2022**, *61*, 227−235.
37. Deng, W.; Yao, C.-Y.; Chen, Y.-C.; Zhou, Y.-Q.; Du, S.-N.; Liu, J.-L.; Tong, M.-L., Engineering a high-barrier d-f single-molecule magnet centered with hexagonal bipyramidal Dy(III) unit. *Sci. China Chem.* **2024,** *67* (10), 3291-3298.

 doi:10.20944/preprints202504.0476.v1

38. Zhong, X.; Li, D.-Y.; Cao, C.; Luo, T.-K.; Hu, Z.-B.; Peng, Y.; Liu, S.-J.; Zheng, Y.-Z.; Wen, H.-R., Effect of Substituents in Equatorial Hexaazamacrocyclic Schiff Base Ligands on the Construction and Magnetism of Pseudo D_{6h} Single-Ion Magnets. *Inorg. Chem.* **2024,** *63* (46), 21909-21918.
39. Armenis, A. S.; Mondal, A.; Giblin, S. R.; Raptopoulou, C. P.; Psycharis, V.; Alexandropoulos, D. I.; Tang, J.; Layfield, R. A.; Stamatatos, T. C., Unveiling new [1+1] Schiff-base macrocycles towards high energy-barrier hexagonal bipyramidal Dy(III) single-molecule magnets. *Chem. Commun.* **2024,** *60* (87), 12730-12733.